Available online at https://link.springer.com/journal/42241
http://www.jhydrodynamics.com
Journal of Hydrodynamics, 2024, 36(3): 556-569
https://doi.org/10.1007/s42241-024-0033-7

Prediction of bedload transport inside vegetation canopies with natural morphology

Li He[1], Yu-qi Shan[1, 2], Chao Liu[1*], Hui Cao[3, 4], Xing-nian Liu[1], Yakun Guo[5]
1. *State Key Laboratory of Hydraulics and Mountain River Engineering, Sichuan University, Chengdu 610065, China*
2. *Institute for Disaster Management and Reconstruction, Sichuan University, Chengdu 610065, China*
3. *China Yangtze Power Co., Ltd., Yichang 443002, China*
4. *Hubei Key Laboratory of Intelligent Yangtze and Hydroelectric Science, Yichang 443002, China*
5. *Faculty of Engineering and Informatics, University of Bradford, Bradford, UK*

(Received February 23, 2024, Revised April 24, 2024, Accepted May 12, 2024, Published online July 5, 2024)

Abstract: Due to vegetation drag and vegetation-generated turbulence, bedload transport in vegetated channels is more complicated than that in nonvegetated channels. It is challenging to obtain accurate predictions of bedload transport in vegetated channels. Previous studies generally used rigid circular cylinders to simulate vegetation, and the impact of plant morphology on bedload transport was typically ignored, these methods deviate from natural scenarios, resulting in prediction errors in transport rates of more than an order of magnitude. This study measured bedload transport rates inside *P. australis*, *A. calamus* and *T. latifolia* canopies and in arrays of rigid cylinders for comparison. The impact of plant morphology on bedload transport in vegetated channels was examined. Inside the canopies of natural morphology, the primary factor driving bedload transport is the near-bed turbulent kinetic energy (TKE), which consists of both bed-generated and vegetation-generated turbulence. A method was proposed to predict the near-bed TKE inside canopies with natural morphology. For the same solid volume fraction of plants, the transport rate inside canopies with a natural morphology is greater than or equal to that within an array of rigid cylinders, depending on the plant shape. This finding indicates that plant morphology has a significant impact on transport rates in vegetated regions and cannot be ignored, which is typical in practice. Four classic bedload transport equations (the Meyer-Peter-Müller, Einstein, Engelund and Dou equations), which are suitable for bare channels (no vegetation), were modified in terms of the near-bed TKE. The predicted near-bed TKE was inserted into these four equations to predict the transport rate in canopies with natural morphology. A comparison of the predictions indicated that the Meyer-Peter-Müller equation had the highest accuracy in predicting the transport rate in vegetated landscapes.

Key words: Vegetated landscapes, turbulent kinetic energy (TKE), bedload transport, plant morphology, predictive methods

0. Introduction

Aquatic vegetation grows in wetlands and plays a crucial ecological role in maintaining wetland ecosystems[1-9]. Wetlands are the most important ecosystems worldwide, however, they have been severely threatened and damaged in recent decades. Human activities (such as infrastructure construction and sand mining) have significantly reduced the sediment supply to wetland systems, resulting in substantial degradation. Approximately 50% of wetlands worldwide have experienced different extents of degradation[10]. Wetlands in rivers, marshes, and coastal regions are important habitats for aquatic vegetation, which have been disappearing at a rate of 1% to 7% annually, resulting in the loss of aquatic vegetation[11-15]. One of the main reasons for wetland degradation is sediment loss and bed erosion associated with the sediment transport rate.

To mitigate wetland degradation, the Ramsar Convention on Wetlands, which was adopted in Ramsar (Iran) in 1971 and began in 1975, aims to prevent the loss of wetlands for breeding and wintering waterfowl. The convention advocates "wise use" to protect wetland ecosystems worldwide. Since China's accession to the convention in January 1992, many policies and legal documents, such as the

Project supported by the National Key Research and Development Program of China (Grant No. 2022YFE0128200), the National Natural Science Foundation of China (Grant Nos. 52379072, 52022063).
Biography: Li He (1998-), Male, Master Candidate,
E-mail: heli000sky@163.com
Corresponding author: Chao Liu,
E-mail: chaoliu@scu.edu.cn

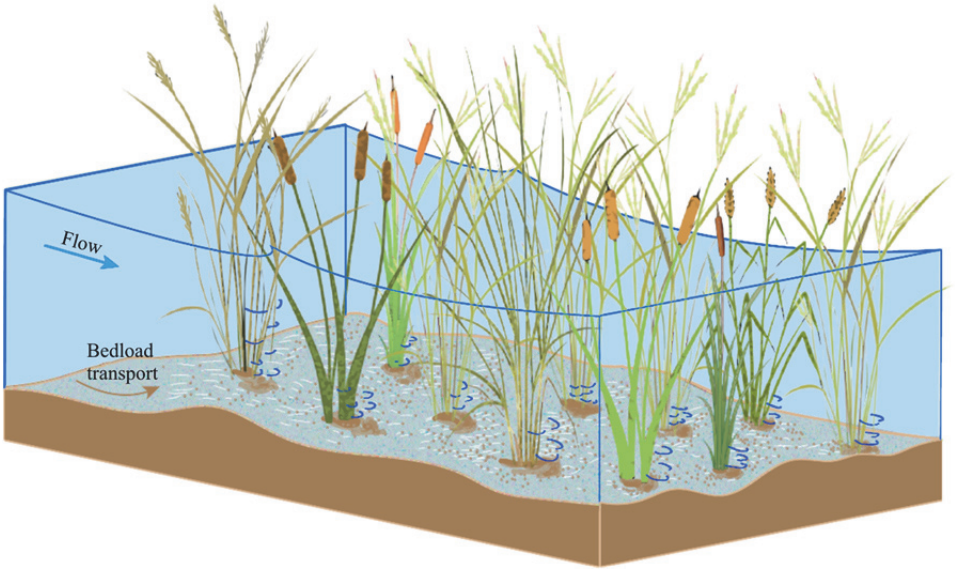

Fig. 1 (Color online) Flow and bedload sediment transport within an emergent vegetation canopy with a natural morphology. *P. australis*, *A. calamus* and *T. latifolia* are commonly observed in aquatic environments

Strengthening Protection and Management of Wetlands, the National Wetland Protection Plan (2022-2030), and the Wetlands Conservation Law, have been enacted. A cross-departmental National Compliance Committee was established to enhance the restoration and management of 82 internationally important wetlands and more than 600 wetland nature reserves in China, and important findings were obtained as a result.

Sediment is a key driver of the morphological evolution of rivers, marshes and coastal areas, and sediment loss is an important factor in wetland degradation. River wetland restoration projects in the Yangtze River and the Mississippi River consider transporting sediment into eroded wetland areas to mitigate wetland degradation[16]. The key factors in restoring wetlands are to effectively evaluate sediment transport and promote sediment deposition. In wetlands, the sediment balance is related to sediment transport and deposition, and precise predictions of sediment transport are important for estimating sediment retention and landscape evolution[17].

Wetlands include both nonvegetated regions (bare beds) and vegetated regions. Previous studies have extensively investigated bedload transport in bare channels (not vegetated) and proposed several methods for predicting the transport rate[18]. However, these methods cannot be directly applied in vegetated regions because vegetation generates additional turbulence that also contributes to bedload transport. That is, traditional bed shear stress-based equations may not be suitable for vegetated regions. Because accurate assessments of bedload transport rates in vegetated regions are important for evaluating the success of wetland restoration projects, this study focused on how to precisely assess transport rates in vegetated regions (Fig. 1).

For nonvegetated regions, previous studies have focused on the impact of bed shear stress (τ) on the bedload transport rate (Q_s). Several classical equations have been proposed for predicting transport rates; for example, the Meyer-Peter-Müller equation[18], the Einstein equation[19], the Engelund equation[20], and the Dou equation[21] are listed as follows:

(1) Meyer-Peter-Müller equation

$$Q_s^* = 8(\theta - \theta_{cr})^{1.5} \tag{1}$$

where Q_s^* is the dimensionless transport rate, θ is the Shield's parameter (with the critical Shield's parameter θ_{cr}).

(2) Einstein equation

$$Q_s^* = 2.15\mathrm{e}^{-0.391/\theta}, \quad \theta < 0.18 \tag{2a}$$

$$Q_s^* = 40\theta^3, \quad 0.18 < \theta < 0.52 \tag{2b}$$

(3) Engelund equation

$$Q_s^* = \frac{9.3}{\beta}(\theta - \theta_c)\left(\sqrt{\theta} - 0.7\sqrt{\theta_c}\right) \tag{3}$$

where Engelund suggested $\beta = 0.8$.

(4) Dou equation

$$Q_s^* = 4.564\theta^2 - \theta^{1.5} \tag{4}$$

The above four traditional equations provide hydraulic engineers with effective methods for predicting the transport rate in the bare channel. In the vegetated region of wetlands, when the velocity is sufficiently large to produce a stem Reynolds number Re_d greater than the critical Reynolds number[22], vegetation generates wake vortices and elevates stem-scale turbulence, which enhances bedload transport[23]. Note that the bed shear stress-based bedload transport equations (Eqs. (1)-(4)) do not include the impact of vegetation on bedload transport, such that a significant underestimation of transport rates by these bed shear stress-based equations was reported in vegetated regions[23-24]. In comparison with bed shear stress, Yang and Nepf [25], Shan et al.[4] found that turbulent kinetic energy (TKE) is the key factor driving sediment transport in vegetated regions. Therefore, a TKE-based sediment transport rate model was proposed by combining the Einstein equation with the TKE model. Next, Zhao and Nepf[26] combined the TKE model with the Meyer-Peter-Müller equation to predict the transport rate in vegetated regions. However, it is still unclear which equation has the best prediction accuracy. One goal of this study was to verify the best prediction equation for the transport rate in vegetated regions.

Although previous studies[23, 25] have provided insights into bedload transport in vegetated regions, these approaches are valid only for circular cylinder arrays. In natural environments, vegetation contains many species, and each of them is unique. The impact of plant morphology on flow structure (velocity and TKE) has been examined[7, 27-28]. However, the impact of plant morphology on bedload transport was not considered in the prediction, and approaches that are valid for cylinder arrays may not be suitable for inside canopies with natural morphology.

To address these knowledge gaps, this study measured bedload transport inside canopies with natural morphology. Three typical species of wetland plants were considered: *P. australis*, *A. calamus* and *T. latifolia*. Transport rates inside these canopies were compared. A method was modified to predict near-bed TKE in vegetated regions with natural plant morphology. By combining the near-bed TKE equation with the four bedload transport equations (Eqs. (1)-(4)), the four new transport rate methods for predicting transport rates in vegetated regions were compared, and the method with the best prediction performance was verified.

1. Theory

1.1 *Prediction of TKE in vegetated regions with natural plant morphology*

Traditional methods for predicting bedload transport rates include bed shear stress (τ)-based approaches, such as the Meyer-Peter-Müller equation (Eq. (1)). In an array of cylinders, the near-bed TKE was the same as the spatial mean TKE, and the difference between the near-bed TKE and spatial mean TKE was ignored. However, this assumption is not valid for plants with natural morphology. Plants with vertically varying plant morphologies produce different TKE values with respect to flow depth, and the TKE in the near-bed region is different from that above. This study focused on the near-bed TKE driving bedload transport in vegetated channels.

The height of the near-bed region was considered $H_{nb} = 5$ cm above the sediment layer. In this region, the velocity and TKE remain approximately constant along the vertical direction, which was confirmed by velocity measurements and Liu et al.[7]. Bedload transport is highly relevant to TKE in the near-bed region. The near-bed TKE, $k_{t(\mathrm{nb})}$, comprises two components: (1) The TKE generated by the channel bed, $k_{t(\mathrm{bed})}$. (2) The TKE generated by vegetation, $k_{t(\mathrm{veg})}$. The prediction of the near-bed TKE, $k_{t(\mathrm{nb})}$, is given as follows

$$k_{t(\mathrm{nb})} = k_{t(\mathrm{veg})} + k_{t(\mathrm{bed})} \tag{5}$$

The bed-generated turbulence is $k_{t(\mathrm{bed})} = \tau_b / \omega$, where τ_b is the bed shear stress, ω is the dimensionless parameter. In this study, the near-bed velocity U_{nb} and near-bed Reynolds shear stress, $\tau_{xz} = -\rho\overline{u'v'}$, where τ_{xz} is approximately the same as τ, were measured to determine, and the dimensionless parameter ω was adopted from a previous study as $\omega = 0.20 \pm 0.01$ [29]. The vegetation-generated turbulence $k_{t(\mathrm{veg})}$ is given as follows

$$k_{t(\mathrm{nb})} = \frac{C_f U_{\mathrm{nb}}^2}{\omega} \tag{6}$$

The vegetation-generated TKE, $k_{t(\mathrm{veg})}$, is related to the stem Reynolds number (Re_d). Vegetation-generated turbulence occurs only when $Re_d > 120$ [22]. Inside canopies of *P. australis*, *A. calamus* and *T. latifolia* and arrays of cylinders, $Re_d = 1\,520$-$2\,080$, suggesting that vegetation-generated turbulence was present in all vegetation canopy cases. Tanino and Nepf[30] proposed the following vegetation-generated TKE prediction

$$k_{t(\mathrm{veg})} = \gamma^2 \left[C_d \frac{n d_e^2}{2(1-\phi)} \right]^{2/3} U_{\mathrm{nb}}^2 \tag{7}$$

where γ is the scale parameter, d_e is the equivalent diameter of vegetation in the near-bed region, n is the plant number per bed area and ϕ is the solid volume fraction. Note that the equivalent diameter was not used to calculate the solid volume fraction for plants with naturally vertically varying morphologies. For rigid cylinders with a vertically uniform morphology, ϕ was determined by the cylinder diameter. However, for the three model plants (*P. australis*, *A. calamus* and *T. latifolia*) with vertically varying morphologies, ϕ was determined by the displacement method. Specifically, the water volume displacing the plant volume (V_v) of a single plant under the water depth (H) was measured such that the solid volume fraction per bed area was ϕ. The form drag coefficient was estimated from $C_d = 2[(0.46 \pm 0.11) + (3.8 \pm 0.5)]$. Note that the development of wake turbulence behind each plant was not restricted if the spacing between vegetation (s) was greater than the diameter of the vegetation (d), therefore, Eq. (7) was valid at $s > d$ [30]. When $s < d$, Eq. (7) is no longer the correct expression of the vegetation-generated TKE. The near-bed TKE in vegetated regions can be predicted by combining Eqs. (5)-(7) such that the prediction of near-bed TKE inside the vegetation canopy is given as follows

$$k_{t(\mathrm{nb})} = \frac{C_f U_{\mathrm{nb}}^{\ 2}}{\omega} + \gamma^2 \left[C_d \frac{n d_e^{\ 2}}{2(1-\phi)} \right]^{2/3} U_{\mathrm{nb}}^{\ 2} \tag{8}$$

The scale parameter γ^2 is related to plant morphology (also the plant frontal area). Tanino and Nepf[30] reported that $\gamma^2 = 1.1 \pm 0.2$ for rigid cylinders, Xu and Nepf[31] reported that $\gamma^2 = 1.6 \pm 0.4$ for *T. latifolia*, and Liu[7] reported that $\gamma^2 = 1.3 \pm 0.2$ for *P. australis*. Considering the uncertainty in γ^2 across all these studies, for simplicity, this study considered $\gamma^2 = 1.2$ for rigid cylinders and three kinds of model plants (*P. australis*, *A. calamus* and *T. latifolia*).

1.2 *Prediction of the bedload transport rate inside canopies with natural morphology*

Because the near-bed TKE is the main controlling factor in bedload transport in vegetated regions, the bed shear stress models for bedload transport rates (Eqs. (1)-(4)) fail to produce satisfactory predictions. Based on the relationship of Soulsby[29], the bed shear stress was replaced by the near-bed TKE

$$k_{t(\mathrm{nb})} = \frac{5.3\tau}{\rho} \tag{9}$$

Equation (9) has been confirmed to be valid in both bare beds and vegetated regions[25, 6, 9, 32].

Using the Shield's parameter θ, Eq. (9) is rewritten as follows

$$k_{t(\mathrm{nb})} = \frac{5.3\theta(\rho_s - \rho)g d_s}{\rho} \tag{10}$$

According to Eq. (10), Eqs. (1)-(4) were modified to predict the bedload transport inside canopies based on the near-bed TKE, which are shown below:

(1) Modified Meyer-Peter-Müller equation

By combining Eq. (1) with Eq. (10), one obtains the following expression

$$Q_s^* = 0.66[k_{t(\mathrm{nb})}^{\ *} - k_{t,cr}^{\ *}]^{1.5} \tag{11}$$

where Q_s^* is the dimensionless bedload transport rate, and the dimensionless near-bed TKE is defined as $k_{t(\mathrm{nb})}^{\ *}$, according to Eq. (9). The dimensionless critical TKE, $k_{t,cr}^{\ *}$, corresponds to sediment initiation[33], based on sediment size.

(2) Modified Einstein equation

By combining Eq. (2) with Eq. (10), one obtains the following expression:

$$Q_s^* = 2.15\mathrm{e}^{-2.06/k_{t(\mathrm{nb})}^{\ *}}, \quad k_{t(\mathrm{nb})}^{\ *} = \frac{k_{t\,(\mathrm{nb})}}{(\rho_s/\rho - 1)g d_s} < 0.95 \tag{12a}$$

$$Q_s^* = 0.27 k_{t(\mathrm{nb})}^{\ *3}, \quad 0.95 < k_{t(\mathrm{nb})}^{\ *} < 2.74 \tag{12b}$$

(3) Modified Engelund equation

By combining Eq. (3) with Eq. (10), one obtains the following expression

$$Q_s^* = 0.95(k_{t(\mathrm{nb})}^{\ *} - k_{t,cr}^{\ *})\left(\sqrt{k_{t(\mathrm{nb})}^{\ *}} - 0.7\sqrt{k_{t,cr}^{\ *}}\right) \tag{13}$$

(4) Modified Dou equation

By combining Eq. (4) with Eq. (10), one obtains the following expression

$$Q_s^* = 0.162 k_{t(\mathrm{nb})}^{\ *2} - \frac{k_{t(\mathrm{nb})}^{\ *1.5}}{12.2} \tag{14}$$

This study aimed to verify the efficacy of four TKE-based methods in vegetated regions, particularly inside emergent canopies with natural morphology (*P. australis*, *A. calamus* and *T. latifolia*).

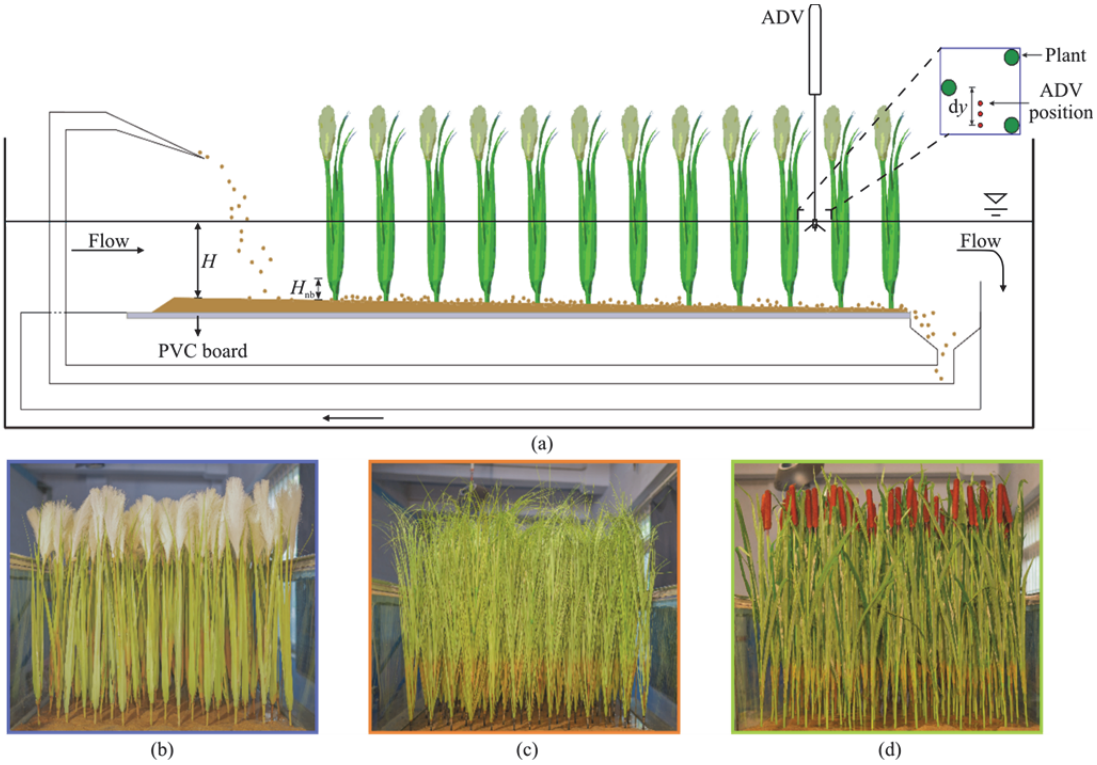

Fig. 2 (Color online) (a) Schematic of the flow and sediment-recirculating flume with a canopy of *P. australis*. The near-bed velocity was recorded in the near-bed region with a height of $H_{nb} = 5$ cm using acoustic Doppler velocimetry. Velocity was measured within a representative unit between two plants at $y = 0$, $y = dy/3$ and $y = 2dy/3$ in the fully developed flow region, where dy is the lateral distance between two side-by-side plants in the middle of two rows in the fully developed flow region inside each canopy. The mean of the measured velocities was used to capture the heterogeneity of the lateral flow. (b) *P. australis* canopy. (c) *A. calamus* canopy and (d) *T. latifolia* canopy

2. Methods

2.1 *Experimental setup*

The experiments were performed in a 17 m long and 1 m wide water-sediment circulation flume with a horizontal bed. The flow meter measured the flow rate (Q), and rulers positioned along the channel measured the water depth (H). Despite slight variations in Q with changes in vegetation density, the water depth remained constant $(H = 20\,\text{cm})$. The entire flume bed was lined with PVC boards with 1 cm thick predrilled, staggered holes. Model plants were glued into the holes of the PVC boards in a staggered arrangement. The test region covered with vegetation was 4 m long and 1 m wide. The entire channel bed was covered by eleven 1.5 m long and 1 m wide PVC boards. Preliminary experiments confirmed that flow fully developed at $x \geq 1.5$ from the leading edge of the canopy. A schematic of the experimental flume with a vegetation canopy (taking *T. latifolia* as an example) is shown in Fig. 2. Five series (A-E) of experiments were performed. Specifically, case A1 is the control for evaluating the transport rate in the bare channel (no vegetation). In Cases B1-B5, the transport rates in arrays of cylinders with a diameter of $d = 0.8$ cm were measured. The cylinders had a vertically uniform morphology. Series C, D and E measured the transport rate inside the canopies of *P. australis*, *A. calamus* and *T. latifolia*. The heights of *P. australis*, *A. calamus* and *T. latifolia* and the cylinders were 77 cm-80 cm, 95 cm-97 cm, 93 cm-96 cm and 30 cm, which were greater than the flow depth $(H = 20\,\text{cm})$, thus, emergent plants were observed in all the cases. When examining the change in bedload transport inside canopies with different morphologies, three kinds of model plants with morphologies very similar to those of real plants were considered (Figs. 2(b)-2(d)). Three species of model plants were produced by a local company based on the plant height, stem width, leaf flexibility and morphology of natural plants. Natural plants were not used because the series of experiments took approximately eight months, which was too long to keep natural plants alive in the experimental flume. To explore the impact

Table 1 Experimental parameters

Plant species	Case	U_d/(cm·s^{-1})	H/cm	ϕ	n/m^{-2}	a_d/ m^{-1}
Bare bed (no vegetation)	A1	25	20	0	0	0
Circular cylinders	B1	25	20	0.0031	60	0.48
	B2	26	20	0.0056	113	0.90
	B3	19	20	0.0082	163	1.30
	B4	22	20	0.0120	239	1.91
	B5	24	20	0.0200	398	3.18
P. australis	C1	22	20	0.0031	44	1.12
	C2	24	20	0.0057	82	2.08
	C3	20	20	0.0080	114	2.90
	C4	23	20	0.0125	179	4.55
A. calamus	D1	25	20	0.0028	40	0.73
	D2	25	20	0.0052	74	1.35
	D3	27	20	0.0071	102	1.86
	D4	22	20	0.0113	161	2.93
T. latifolia	E1	22	20	0.0026	40	0.36
	E2	21	20	0.0048	74	0.67
	E3	21	20	0.0066	102	0.92
	E4	25	20	0.0105	161	1.45

Note: U_d is the depth-averaged velocity, H is the flow depth, ϕ is the solid volume fraction, n is the vegetation density and a_d is the depth-averaged frontal area over the entire flow depth.

of vegetation density on the near-bed TKE and bedload transport rate, different density ranges were considered for the three species of plants. For rigid cylinders (B1-B5), the vegetation density was $n = 60$ plants / m^{-2} - 398 plants / m^{-2}, corresponding to the plant frontal area per unit canopy volume $a = 0.5$ m^{-1} - 3.2 m^{-1}, and the vegetation solid volume fraction $\phi = 0.0031 - 0.02$. *P. australis* (C1-C4) had a density range of $n = 44$ plants / m^2 - 179 plants / m^2, with a frontal area of $a = 0.48$ m^{-1} - 3.19 m^{-1} and a solid volume fraction of $\phi = 0.0031 - 0.0134$. *A. calamus* (D1-D4) had a density range of $n =$ 40 plants / m^2 - 161 plants / m^2, with a frontal area of $a = 0.5$ m^{-1} - 2.9 m^{-1} and a volume fraction of $\phi =$ $0.0028 - 0.0113$. *T. latifolia* (E1-E4) had a density range of $n = 44$ plants / m^2 - 179 plants / m^2, with a frontal area of $a = 0.5$ m^{-1} - 1.9 m^{-1} and a volume fraction of $\phi = 0.0026 - 0.0105$. The densities of *P. australis*, *A. calamus* and *T. latifolia* were chosen based on the range of $\phi = 0.001 - 0.02$ in field studies[34-36]. The experimental parameters used in each case are summarized in Table 1.

At the beginning of each experiment, a 5 cm thick layer of sand was placed on top of the PVC boards and flattened manually. The sediment had a median grain size of $d_{50} = 0.5$ mm and a density of $\rho_s = 2.65$ g/cm^3. The bedload transport rate (Q_s) was measured by a mesh bag with holes smaller than 0.25 mm at the exit of the sediment recirculating pipe. The collected wet sediment was placed into a measuring cup with a measured volume of water. The total volume (V_{tot}) and mass (m_{tot}) of the water and sediment were recorded, where $V_{\text{tot}} = V_w + V_s$, $m_{\text{tot}} = \rho_w V_w + \rho_s V_s$. The grain volume ($V_s$) was calculated as $V_s = (m_{\text{tot}} - \rho_w V_{\text{tot}}) / (\rho_s - \rho_w)$. The bedload transport rate (Q_s) per channel width was calculated by the following equation

$$Q_s = \frac{\rho_s V_s}{W \Delta T} \tag{15}$$

where W is the flume width, ΔT is the sediment collection time. ΔT was set based on the mean channel velocity and ranged from 60 s to 120 s. Sediment transport rates were measured every two hours until the current measurement was the same as the previous one within uncertainty. This fact indicated that bedload transport had reached equilibrium. For each case, a minimum run time of 14 h and up to 36 h were needed.

2.2 *Velocity measurements*

The x-, y- and z-coordinates were defined as the longitudinal, lateral and vertical directions, respectively. $x = 0$ was the value set for the leading edge of the canopy, $y = 0$ was the value set for the centerline of the vegetated region, and $z = 0$ was the value set for the bed surface. After the transport rate reached equilibrium, the acoustic Doppler velocimeter (ADV) with a downward-looking probe was fixed to a positioning system across the flume, and the ADV could move in the x-, y- and z-directions. The ADV measured the instantaneous flow velocities $u(t)$, $v(t)$ and $w(t)$ along the vertical direction in the near-bed region. At each position, the velocity was measured at a frequency of 50 Hz for 240 s. The raw velocity data with correlations smaller than 80% and a signal-to-noise ratio less than 15 were filtered and despiked using the method described in Goring and Nikora[37]. Specifically, the approach employed herein utilizes the three-dimensional phase-space plot paradigm to delineate an ellipsoid encompassing residual velocities and their corresponding derivatives. Observations exterior to this ellipsoidal boundary are defined as spikes. An iterative methodology is adopted to iteratively diminish the dimensions of the ellipsoid to identify spikes, and this process is continued until subsequent spike replacement iterations yield negligible effects. Subsequently, eradicated spikes are substituted via third-order cubic spline interpolation. The remaining instantaneous velocities were processed using Matlab to obtain the time-averaged velocities $(\overline{u},\overline{v},\overline{w})$ and the instantaneous fluctuating velocities (u',v',w'). Finally, the turbulent kinetic energy, k, was defined as $k = 0.5(\overline{u'^2} + \overline{v'^2} + \overline{w'^2})$.

At each measurement point, a representative region (Fig. 2(a)) was considered. Velocities were measured in the fully developed flow region in the middle of two rows and in three locations in a representative region between two plants (inset plot in Fig. 2): $y = 0$, $\mathrm{d}y/3$ and $2\mathrm{d}y/3$, where $\mathrm{d}y$ is the lateral distance between two side-by-side plants. The mean velocity in the representative region was defined as $U\,(=(\sum_1^3 u)/3)$, and the TKE was defined as $k_t\,(=(\sum_1^3 k)/3)$. This process was used to capture the heterogeneity of lateral flow between plants. For the representative region in each canopy, the depth-averaged velocity was defined as $U_d = 1/H\int_0^H U(z)\mathrm{d}z$. The region beneath the leaves was consi- dered as the near-bed region ($0\,\mathrm{cm} < z < 5\,\mathrm{cm}$, $H_{\mathrm{nb}} = 5\,\mathrm{cm}$), where the frontal area, streamwise velocity and TKE remained constant along the vertical direction. The near-bed velocity was $U_{\mathrm{nb}}\,(=1/H_{\mathrm{nb}}\int_0^{H_{\mathrm{nb}}} U(z)\mathrm{d}z)$, and the near-bed TKE was $k_{t\,(\mathrm{nb})}\,(=1/H_{\mathrm{nb}}\int_0^{H_{\mathrm{nb}}} k_t(z)\mathrm{d}z)$.

To quantitatively compare predictions and measurements, the mean relative error (MRE) was defined as follows

$$\mathrm{MRE} = \frac{1}{N}\sum\frac{|X_P - X_M|}{X_M} \tag{16}$$

where N is the number of predictions and measurements, X_P and X_M is the prediction and measurement.

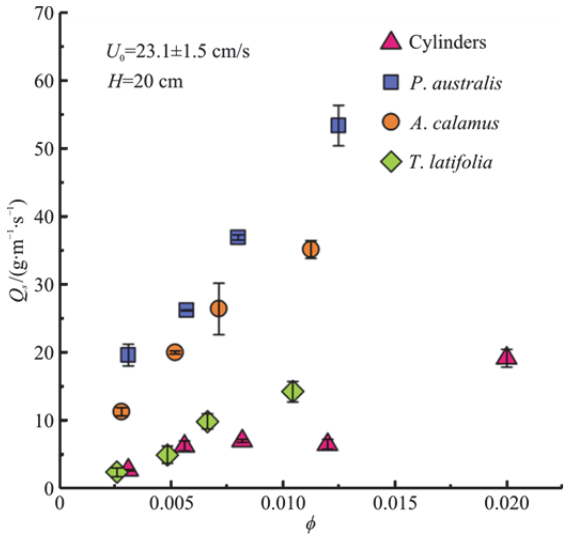

Fig. 3 (Color online) Measured sediment transport rates (Q_s) versus solid volume fraction (ϕ) for three species of plants (*P. australis*, *A. calamus* and *T. latifolia*) and cylinder arrays. The flow conditions were a mean channel velocity of $U_0 = 23.1 \pm 1.5$ cm/s and a flow depth of $H = 20$ cm. Transport rates in cylinder arrays were used for comparison

3. Results

3.1 *Bedload transport inside canopies*

The impacts of plant density (ϕ) and plant morphology on the bedload transport rate (Q_s) inside canopies were examined (Fig. 3). For the same channel mean velocity and flow depth ($U_0 = 23.1 \pm 1.5$ cm/s, $H = 20$ cm), a larger ϕ provided higher Q_s values for both cylinders and model vegetation with natural morphology (*P. australis*, *A. calamus* and *T. latifolia*). For different solid volume fractions (ϕ), greater vertical variation in plant morphology (e.g., *P. australis*, blue squares in Fig. 3) produced a greater near-bed TKE relative to that of

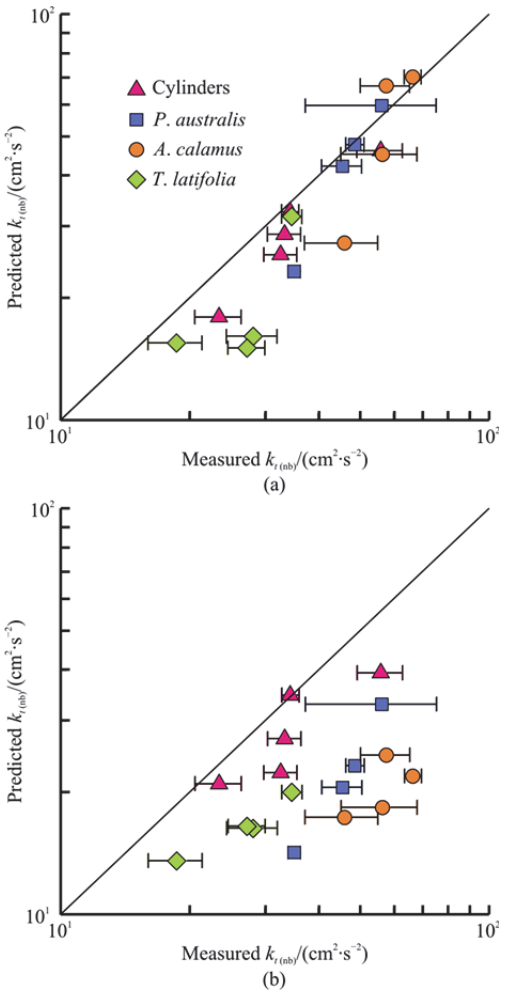

Fig. 4 (Color online) Comparison between the predicted near-bed TKE and measurements inside canopies with real morphology and arrays of rigid cylinders. (a) Predicted TKE, $k_{t(\mathrm{nb})}$, estimated from Eq. (8) using the measured near-bed velocity U_{nb} against the measured $k_{t(\mathrm{nb})}$, (b) Predicted TKE, $k_{t(\mathrm{nb})}$, estimated from Eq. (8) using the measured depth-averaged velocity U_d against the measured $k_{t(\mathrm{nb})}$

cylinders (red triangles in Fig. 3). The bedload transport rates for *P. australis* (blue squares) and *A. calamus* (orange circles) are significantly greater than those for cylinders (red triangles) and *T. latifolia* (green diamonds). At $\phi = 0.0031$, the transport rates of *T. latifolia* ($Q_s = 2.5 \pm 0.7$ g/m/s) and of the cylinders ($Q_s = 2.8 \pm 0.1$ g/m/s) were comparable because the morphology of *T. latifolia* exhibited little vertical variation. In contrast, the morphology of *P. australis* and *A. calamus* varied significantly along the vertical direction. There were considerable impacts of two species (*P. australis* and *A. calamus*) on the near-bed flow structure (velocity and TKE), and the transport rates in *P. australis* and *A. calamus* were 5-11 and 2-5 times greater than those in the arrays of cylinders, respectively. Considering the same solid volume fraction (ϕ), this finding suggests that bedload transport rates measured in cylinder arrays significantly differ from those measured in canopies with natural morphology. The influence of plant morphology on bedload transport rates cannot be ignored in vegetated channels. In particular, rigid cylinders simulate real plants poorly in natural environments.

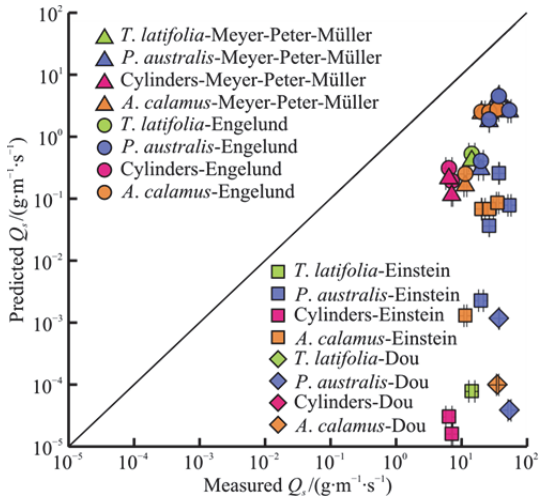

Fig. 5 (Color online) Comparison between the predicted and measured bedload transport rates. The transport rates were predicted using bed shear stress-based approaches (Eqs. (1)-(4)) and were underestimated by magnitudes (~10-10^5). The triangles, squares, circles, and diamonds represent the results of the Meyer-Peter-Müller, Einstein, Engelund, and Dou equations (Eqs. (1)-(4))

3.2 *Prediction of near-bed TKE inside canopies*

The experimental data in this study (Series A-E in Table 1) were used to estimate the near-bed TKE inside canopies, i.e., Eq. (8). Using measured near-bed velocities, the predicted near-bed TKE agreed well with the measurements (Fig. 4(a)), with a mean relative error less than 19%. This finding suggests that Eq. (8) provides a reasonable prediction of the near-bed TKE inside both cylinders and three plants with natural morphology, indicating that it is reasonable to use U_{nb} and d_e to predict the near-bed TKE (considering the impact of plant morphology on the near-bed velocity). When the influence of plant morphology on the near-bed velocity was ignored, the near-bed velocity (U_{nb}) was replaced by the depth-averaged velocity (U_d). Using U_d in Eq. (8), the prediction of near-bed TKE changed slightly in the cylinder arrays; however, the prediction of near-bed TKE in three canopies (*P.* australis, *A.* calamus and *T.* latifolia) was underestimated, with a mean relative

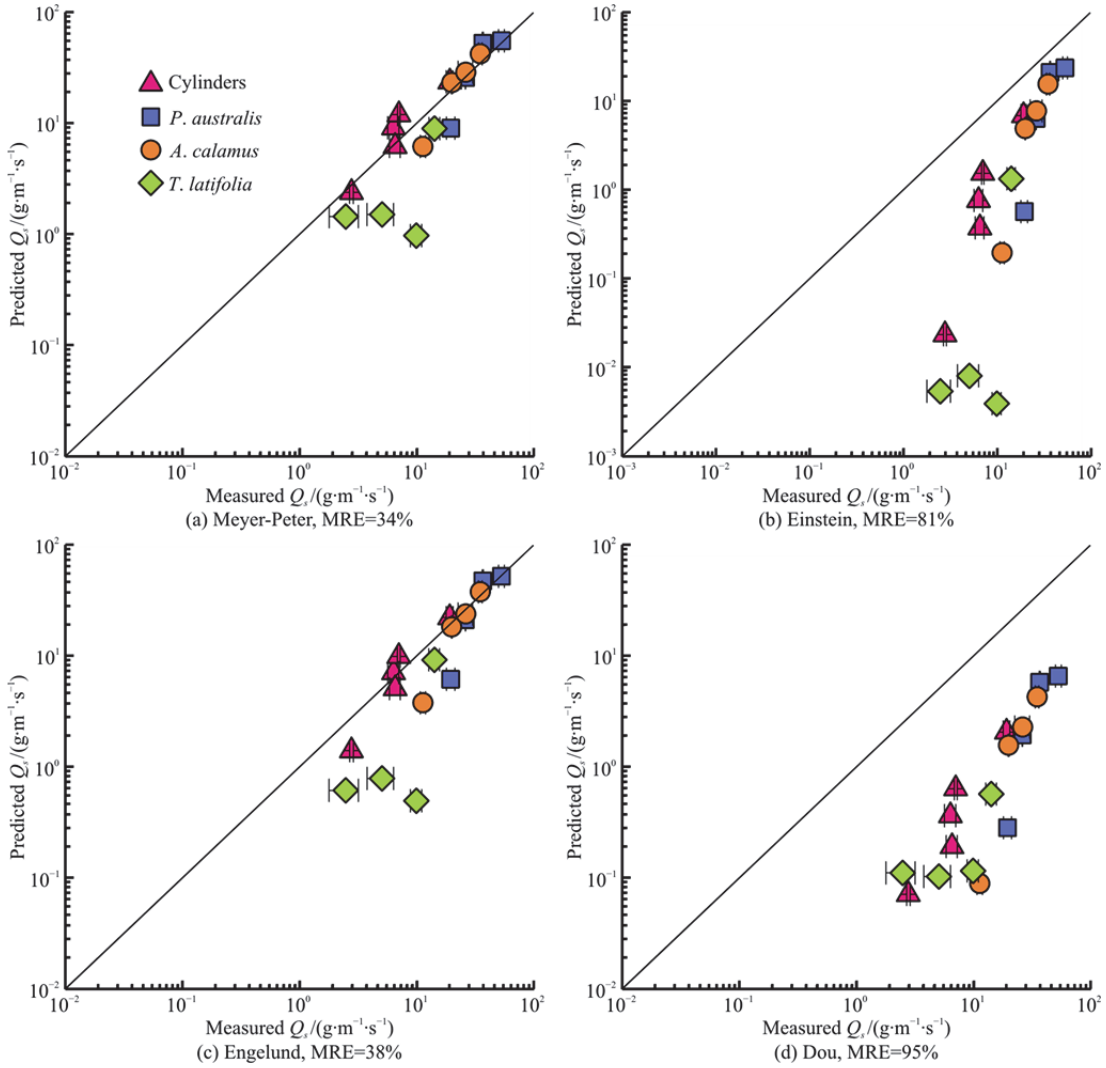

Fig. 6 (Color online) Comparison of the predicted and measured near-bed TKE-based bedload transport rates using the (a) Meyer-Peter-Müller equation, Eq. (11), (b) Einstein equation, Eq. (12), (c) Engelund equation, Eq. (13) and (d) Dou equation, Eq. (14). MRE is the mean relative error, defined in Eq. (16). Among the four methods, the near-bed TKE-based Meyer-Peter-Müller equation has the best performance in predicting the bedload transport rate inside canopies with natural morphology

error increasing to 42% (Fig. 4(b)). Ignoring the effect of plant morphology on near-bed velocity was reasonable for cylinders but not appropriate for plants with natural morphology. Thus, the assumption of $U_d \approx U_{\mathrm{nb}}$ was valid for cylindrical cases but not for canopies with vertically varying morphologies.

3.3 *Comparison of the four TKE-based prediction models*

The predictions of the transport rate by four bed shear stress-based equations (Eqs. (1)-(4)) are compared with the measurements (Fig. 5). The predictions of the four equations were underestimated by order of magnitudes (~10-10^5) for both arrays of cylinders and canopies with natural morphology. This finding confirms that the four τ-based equations are not suitable for predicting transport rates in vegetated regions. Additionally, this comparison suggested that bed shear stress (τ) was not the key factor driving bedload transport in vegetated regions.

Next, the predictions of four TKE-based equations (Eqs. (11)-(14)) were compared to the measurements in the arrays of cylinders and canopies of *P. australis*, *A. calamus, and T. latifolia* (Fig. 6). The predicted near-bed TKE, $k_{t(\mathrm{nb})}$, from Eq. (5) was used in Eqs. (11)-(14) to predict the transport rates. Compared to that of the τ-based model, the prediction accuracy of the proposed model is significantly improved. The predictions for the cylinder arrays and three canopies using the modified Meyer-Peter-Müller equation (Eq. (11)) and the modified Engelund equation (Eq. (13)) agreed with the measurements,

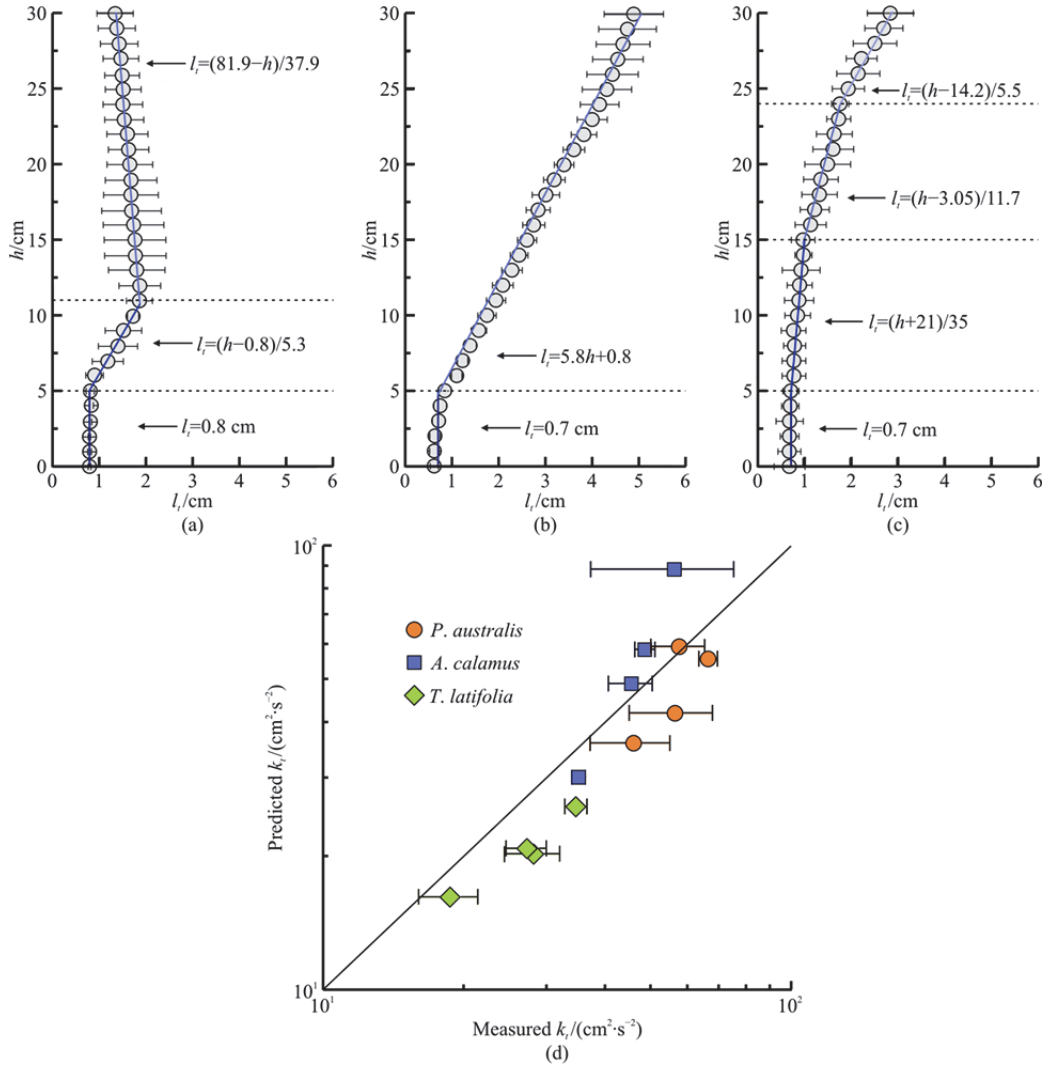

Fig. 7 (Color online) Vertical profiles of the lateral average integral length scale for eddies inside the canopy of (a) *P. australis*, (b) *A. calamus* and (c) *T. latifolia*. The error bar indicates the variability at three different angles. The best fitting lines are denoted by lines with the fitting equations. (d) Comparison between the predicted depth-averaged TKE from Eq. (17) and the measured near-bed TKE, MRE = 24%

with mean relative errors of MRE = 34%, 38% (Figs. 6(a), 6(b)). However, the predictions for the modified Einstein equation (Eq. (12)) and the modified Dou equation (Eq. (14)) were significantly underestimated, with MRE = 81%, 95% (Figs. 6(c), 6(d)). The potential reason for the difference in predictions was that the modified Meyer-Peter-Müller equation (Eq. (11)) and the modified Engelund equation (Eq. (13)) contain the sediment initiation threshold, i.e., the critical Shield's parameter $k_{t,cr}^*$ (also θ_c) in Eqs. (11), (13). Since the critical condition for sediment initiation was included, these two equations have a threshold for evaluating whether bedload transport occurs (i.e., $k_{t,(\mathrm{nb})}^* > k_{t,cr}^*$). However, the modified Einstein equation (Eq. (12)) and Dou equation (Eq. (14)) do not include the sediment initiation threshold, and thus, neither equation has a threshold for evaluating the presence or absence of bedload transport. In particular, for low-flow conditions, bedload transport in vegetated regions may still occur due to additional vegetation-generated turbulence. However, neither the Einstein equation nor the Dou equation can evaluate this phenomenon and may inaccurately capture the bedload transport degree, leading to transport rate underestimations.

Overall, the above comparison suggests that inside the cylinder arrays and canopies of natural morphology, the modified Meyer-Peter-Müller equation (Eq. (11)) combined with the predicted near-bed *TKE* has the highest accuracy among the four equations and is the recommended equation to use for predicting bedload transport in vegetated regions.

4. Discussion

4.1 *Depth-averaged TKE prediction*

The $U_d \approx U_{\mathrm{nb}}$ assumption was valid inside the circular cylinders with a vertically uniform morphology but not within the canopies with a vertically varying morphology (Section 4.2). The depth-averaged TKE prediction over the full-flow depth is used in general, so we discuss the difference between the near-bed TKE, $k_{t(\mathrm{nb})}$ (Eq. (8)), and the depth-averaged TKE, $k_{t(d)}$ (Eq. (17))

$$k_{t(d)} = \frac{C_f U_d^{\,2}}{\omega} + \gamma^2 \left[C_d \frac{a l_{t(d)}}{2(1-\phi)} \right]^{2/3} U_d^{\,2} \tag{17}$$

where $l_{t(d)}$ is the depth-averaged length scale for eddies, C_d is the depth-average form drag coefficient. The value of l_t depends on the plant morphology. For plants with natural morphology (e.g., *P. australis*, *A. calamus* and *T. latifolia*), l_t was not equal to the stem diameter of a single plant. For the near-bed area ($z < 5$ cm), l_t was equal to the diameter of the main stem, d, as leaves exert a negligible influence in this region. Above the near-bed area ($z > 5$ cm), the influence of leaves became significant, such that l_t was defined as the mean width of the leaves. Using the Python image processor, the vertical profiles of l_t were obtained for three plants (Figs. 7(a)-7(c)). The best fitting equation of l_t in Figs. 7(a)-7(c) was used to estimate $l_{t(d)}$.

Using the measured depth-averaged velocities (U_d) and the depth-averaged length scale for eddies, $l_{t(d)}$, the predicted depth-averaged TKE agreed well with the measurements (Fig. 7(d)), with a MRE less than 24%. This finding suggests that Eq. (17) also provides a reasonable depth-averaged TKE prediction inside canopies with natural morphology.

4.2 *Model application*

The proposed near-bed TKE (Eq. (8)) and depth-averaged TKE (Eq. (17)) can be applied under natural conditions. Vegetation conditions (such as vegetation morphology, density, volume fraction, and frontal area) can be obtained by sampling plants in fields. The measured near-bed velocity or the depth-averaged velocity in vegetated regions is used to estimate the near-bed TKE or the depth-averaged TKE. The predicted near-bed TKE or depth-averaged TKE was used to predict the transport rate.

Assuming the same energy slope (S) and water depth (H), the bedload transport rate (Q_s) was predicted over a wide range of solid volume fractions (ϕ) in a marsh filled with *P. australis*. *P. australis* had a diameter of $d = 0.8$ cm, a solid volume fraction of $\phi = 10^{-3}$ - 10^{-1}, a water depth of $H = 20$ cm, an energy slope of $S = 0.015$, and a mean grain size of $d_s = 0.5$ mm, which met the condition of case C2 ($\phi = 0.0057$). Inside the *P. australis* canopy, the balance between bed friction, vegetation drag and flow energy is

$$C_f U^2 + \frac{1}{2(1-\phi)} \rho C_d a H U^2 = \rho g H S \tag{18}$$

The channel-average velocity (U) is obtained as follows

$$U = \sqrt{\frac{gHS}{C_f + \dfrac{C_d a H}{2(1-\phi)}}} \tag{19}$$

We investigate the difference between the prediction of the near-bed TKE (Eq. (8)) and the depth-averaged TKE (Eq. (17)) via the modified Meyer-Peter-Müller equation (Eq. (11)) and the modified Einstein equation (Eq. (12)) using the channel-averaged velocity U. Notably, Eqs. (8), (17) are valid only at $Re_d > 120$. When $U > 10$ cm/s, $Re_d > 800$, vegetation-generated turbulence occurs at all solid volume fractions.

Under the same energy slope, U decreased as ϕ increased due to vegetation drag (Fig. 8(a)). Consistent with this trend, both the near-bed TKE (solid line) and depth-averaged TKE (dashed line) decreased as ϕ increased (Fig. 8(b)). The predicted near-bed TKE was closer to the measured value. The predicted near-bed TKE was greater than the depth-averaged TKE at a small solid volume fraction $\phi (> 0.005)$ because a denser canopy resulted in a stronger impact on the near-bed TKE.

Using the predicted dimensionless near-bed TKE ($k_{t(\mathrm{nb})}^{*}$), the dimensionless bedload transport (Q_s^{*}) was calculated using the modified Meyer-Peter-Müller equation (Eq. (11), red lines) and the modified Einstein equation (Eq. (12), blue lines). Figure 8(c) shows that the transport rates Q_s^{*} predicted by the Meyer-Peter-Müller equation and the Einstein equation decrease as ϕ increases (Fig. 8(c)). Q_s^{*} predicted by the Meyer-Peter-Müller equation was smaller than that predicted by the Einstein equation at $\phi < 0.0016$. When $\phi > 0.0016$, the Meyer-Peter-Müller

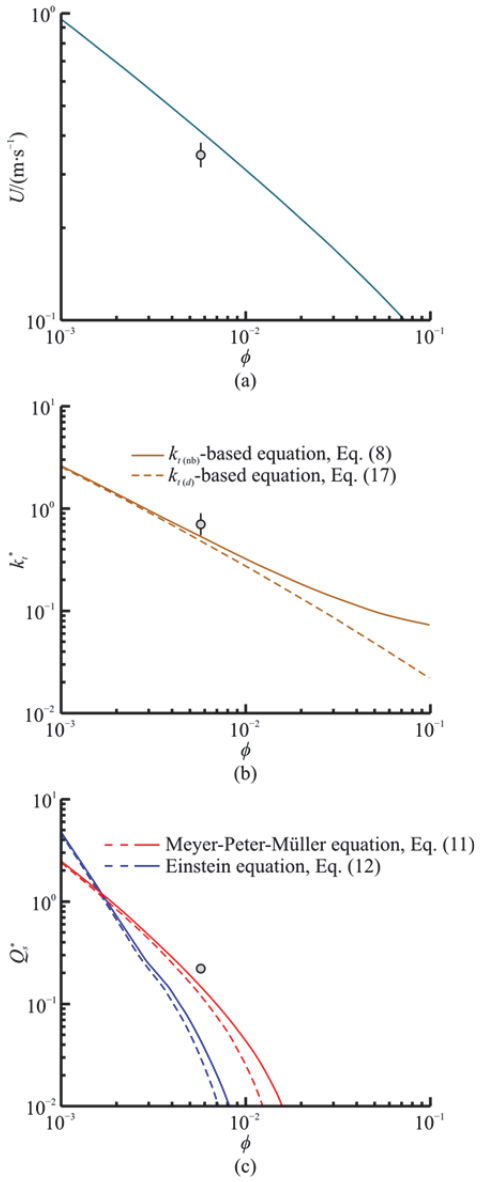

Fig. 8 (Color online) (a) The channel-average velocity U, (b) Dimensionless turbulent kinetic energy k_t^*, predicted by Eq. (8) (orange solid line) and Eq. (17) (orange dashed line) and (c) The dimensionless bedload transport rate Q_s^*, estimated from both the TKE-based Meyer-Peter-Müller equation (red line) and the TKE-based Einstein equation (blue line), as a function of the solid volume fraction ϕ. Solid and dashed lines represent dimensionless TKE k_t^* estimated from Eqs. (8) and (17). The gray circles in the three plots represent the measurements of case C2 at $\phi = 0.0057$

equation produced a greater prediction than the Einstein equation. The comparison indicates that at $\phi = 0.0057$, the $Q_s^*(= 0.16)$ predicted by the Meyer-Peter-Müller equation agreed well with the measured value $(= 0.22)$. Overall, it is recommended to use the modified Meyer-Peter-Müller equation (Eq. (11)) to predict bedload transport in canopies with natural morphology.

4.3 *Model limitations*

The model of the present study is proposed to predict the bedload transport rates inside emergent vegetation canopies. In natural marshes, vegetation may be submerged[38, 17] or floating[39-40], thus, the proposed model may be modified to predict the bedload transport rate inside submerged or floating vegetation. In this study, plant reconfiguration was not observed at a mean channel velocity of $U_0 = 25.1\,\mathrm{cm/s}$. However, in the field, the velocity may increase due to the occurrence of floods, and the plant may be deflected, therefore, the proposed model is not suitable for these situations.

We reiterate that previous studies generally ignored the effect of plant morphology on flow and sediment transport. Estimators of the TKE and transport rate have been proposed for rigid array cylinders[25, 4] that are not suitable for canopies with natural morphologies. This study considered the impact of morphology on the near-bed flow conditions (near-bed velocity and TKE) and transport rate, which filled the research gap of previous studies. The validation in Fig. 6 confirmed that the proposed methods (Eqs. (8), (11)) for predicting the near-bed TKE and transport rate are valid for canopies with natural morphology.

4.4 *Future study*

Current research on flow and sediment transport has been conducted in experimental flumes. Future studies should focus on the gap between laboratory-scale and natural-scale observations. The current experiments considered the vegetated area filled with only one vegetation species, which is not true in natural rivers. Many plant species grow together in shallow flow regions or on river floodplains. There are various types of vegetation, such as rigid and flexible, emergent and submerged vegetation, which makes sediment transport more difficult to predict. Determining how to include the effects of different plant species on flow and sediment transport is challenging.

5. Conclusion

Laboratory experiments were performed to investigate the influence of the vegetation solid volume fraction, plant species, and near-bed TKE on bedload transport inside different emergent canopies of vegetation. This study investigated rigid circular cylinders with a vertically uniform morphology and model plants (*P. australis*, *A. calamus* and *T. latifolia*)

with a natural morphology. The near-bed TKE inside the canopy is the main factor driving bedload transport in vegetated regions. Under the same solid volume fractions (ϕ) and flow conditions (U_0 and H), the bedload transport rates inside canopies with vertically varying morphologies (e.g., *P. australis*, *A. calamus* and *T. latifolia*) were greater than those with vertically uniform morphologies (e.g., rigid cylinders). Plant morphology is an important factor that affects bedload transport rates in vegetated regions and cannot be ignored. Based on the near-bed TKE, a model was proposed to predict bedload transport rates inside canopies with natural morphologies. The predictions agreed with the measurements. The experimental results indicated that the near-bed TKE-based Meyer-Peter-Muller equation accurately predicts transport rates inside canopies with natural morphologies.

Acknowledgment

This work was supported by the Fundamental Research Project of China Yangtze Power Co., Ltd. (Grant No. 2423020045).

Compliance with ethical standards

Conflict of interest: The authors declare that they have no conflict of interest. Chao Liu is editorial board member for the Journal of Hydrodynamics and was not involved in the editorial review, or the decision to publish this article. All authors declare that there are no other competing interests.

Ethical approval: This article does not contain any studies with human participants or animals performed by any of the authors.

Informed consent: Not application.

References

[1] Suding K. N. Toward an era of restoration in ecology: Successes, failures, and opportunities ahead [J]. *Annual Review of Ecology, Evolution, and Systematics*, 2011, 42: 465-487.

[2] Alongi D. M. Carbon cycling and storage in mangrove forests [J]. *Annual Review of Marine Science*, 2014, 6: 195-219.

[3] Zhang Y., Jeppesen E., Liu X. et al. Global loss of aquatic vegetation in lakes [J]. *Earth-Science Reviews*, 2017, 173: 259-265.

[4] Shan Y., Zhao T., Liu C. et al. Turbulence and bed load transport in channels with randomly distributed emergent patches of model vegetation [J]. *Geophysical Research Letters*, 2020, 47(12): e2020GL087055.

[5] Huai W. X., Wang X., Guo Y. et al. Investigation of the sediment transport capacity in vegetated open channel flow [J]. *Journal of Hydrodynamics*, 2021, 33(2): 386-389.

[6] Liu C., Shan Y., Nepf H. Impact of stem size on turbulence and sediment resuspension under unidirectional flow [J]. *Water Resources Research*, 2021, 57(3): e2020WR028620.

[7] Liu C., Yan C., Shan Y. et al. An exponential-based model for predicting velocity fields in partially vegetated channels [J]. *Journal of Hydraulic Research*, 2022, 60(6): 864-879.

[8] Liu Y., Fang H. Z., Yang Z. H. et al. Longitudinal dispersive coefficient in channels with aquatic vegetation: A review [J]. *Journal of Hydrodynamics*, 2023, 35(3): 379-395.

[9] Shan Y., Yan C., Liu J. et al. Predicting velocity and turbulent kinetic energy inside an emergent Phragmites australis canopy with real morphology [J]. *Environmental Fluid Mechanics*, 2023, 23: 943-963.

[10] Wu S., Wang X., Liu T. et al. Research advances of the wetland restoration based on CiteSpace [J]. *Acta Ecologica Sinica*, 2022, 42(3): 1224-1239(in Chinese).

[11] Hu S., Niu Z., Chen Y. et al. Global wetlands: Potential distribution, wetland loss, and status [J]. *Science of the Total Environment*, 2017, 586: 319-327.

[12] Chen H., Zhang W., Gao H. et al. Climate change and anthropogenic impacts on wetland and agriculture in the Songnen and Sanjiang Plain, Northeast China [J]. *Remote Sensing*, 2018, 10(3): 356.

[13] Reid A. J., Carlson A. K., Creed I. F. et al. Emerging threats and persistent conservation challenges for freshwater biodiversity [J]. *Biological Reviews*, 2019, 94(3): 849-873.

[14] Serrano O., Lovelock C. E., Atwood T. B. et al. Australian vegetated coastal ecosystems as global hotspots for climate change mitigation [J]. *Nature Communications*, 2019, 10(1): 4313.

[15] Wang W., Fu H., Lee S. Y. et al. Can strict protection stop the decline of mangrove ecosystems in China? From rapid destruction to rampant degradation [J]. *Forests*, 2020, 11(1): 55.

[16] DuBowy P. J. Mississippi River ecohydrology: Past, present and future [J]. *Ecohydrology and Hydrobiology*, 2013, 13(1): 73-83.

[17] Huai W., Li S., Katul G. G. et al. Flow dynamics and sediment transport in vegetated rivers: A review [J]. *Journal of Hydrodynamics*, 2021, 33(3): 400-420.

[18] Meyer-Peter E., Müller R. Formulas for bed-load transport [C]. *The International Association of Hydro-Environment Engineering and Research 2nd Meeting*, Stockholm, Sweden, 1948.

[19] Einstein H. A. The bed-load function for sediment transportation in open channel flows [R]. US Department of Agriculture, 1950.

[20] Engelund F., Fredsøe J. A sediment transport model for straight alluvial channels [J]. *Hydrology Research*, 1976, 7(5): 293-306.

[21] Dou G. R. A similarity theory concerning the design of total sediment transport models with reference to a particular project [J]. *Hydro-Science and Engineering*, 1977, (3): 1-20(in Chinese).

[22] Liu C., Nepf H. Sediment deposition within and around a finite patch of model vegetation over a range of channel velocity [J]. *Water Resources Research*, 2016, 52(1): 600-612.

[23] Yager E. M., Schmeeckle M. W. The influence of vegetation on turbulence and bed load transport [J]. *Journal of Geophysical Research: Earth Surface*, 2013, 118(3): 1585-1601.

[24] Tinoco R. O., Coco G. Observations of the effect of emergent vegetation on sediment resuspension under unidirectional currents and waves [J]. *Earth Surface Dynamics*, 2014, 2(1): 83-96.
[25] Yang J. Q., Nepf H. M. A turbulence-based bed-load transport model for bare and vegetated channels [J]. *Geophysical Research Letters*, 2018, 45(19): 428-436.
[26] Zhao T., Nepf H. M. Turbulence dictates bedload transport in vegetated channels without dependence on stem diameter and arrangement [J]. *Geophysical Research Letters*, 2021, 48: e2021GL095316.
[27] King A. T., Tinoco R. O., Cowen E. A. A *k-ε* turbulence model based on the scales of vertical shear and stem wakes valid for emergent and submerged vegetated flows [J]. *Journal of Fluid Mechanics*, 2012, 701: 1-39.
[28] Wu Y. J., Jing H. F., Li C. G. et al. Flow characteristics in open channels with aquatic rigid vegetation [J]. *Journal of Hydrodynamics*, 2020, 32(6): 1100-1108.
[29] Soulsby R. L. Measurements of the Reynolds stress components close to a marine sand bank [J]. *Marine Geology*, 1981, 42(1-4): 35-47.
[30] Tanino Y., Nepf H. M. Lateral dispersion in random cylinder arrays at high Reynolds number [J]. *Journal of Fluid Mechanics*, 2008, 600: 339-371.
[31] Xu Y., Nepf H. Measured and predicted turbulent kinetic energy in flow through emergent vegetation with real plant morphology [J]. *Water Resources Research*, 2020, 56(12): e2020WR027892.
[32] Sun S., Shan Y., Yan C. et al. Impact of sediment size, channel velocity and plant density on sediment deposition inside Phragmites australis canopies [J]. *Journal of Hydrology*, 2023, 626: 130151.
[33] Julien P. Y. Erosion and sedimentation [M]. Cambridge, UK: Cambridge University Press, 2010.
[34] Eid E. M., Shaltout K. H., Asaeda T. Modeling growth dynamics of Typha domingensis (Pers.) Poir. ex Steud. in Lake Burullus, Egypt [J]. *Ecological Modelling*, 2012, 243: 63-72.
[35] Ranjan A., Jain P., Singh B. et al. Acorus calamus L.: An insight review of botany, chemistry, medicinal uses and cultural practice [J]. *Journal of Chemical, Biological and Physical Sciences*, 2016, 6(3): 1027.
[36] Zheng Y., Yang D., Dzakpasu M. et al. Effects of plants competition on critical bacteria selection and pollutants dynamics in a long-term polyculture constructed wetland [J]. *Bioresource Technology*, 2020, 316: 123927.
[37] Goring D. G., Nikora V. I. Despiking acoustic Doppler velocimeter data [J]. *Journal of Hydraulic Engineering, ASCE*, 2002, 128(1): 117-126.
[38] Huai W X., Zhang J., Katul G. G. et al. The structure of turbulent flow through submerged flexible vegetation [J]. *Journal of Hydrodynamics*, 2019, 31(2): 274-292.
[39] Gui Z., Shan Y., Liu C. Flow velocity evolution through a floating rigid cylinder array under unidirectional flow [J]. *Journal of Hydrology*, 2023, 617: 128915.
[40] Gui Z., Shan Y., Liu C. Flow velocity adjustment in a channel with a floating vegetation canopy [J]. *Journal of Hydrology*, 2024, 628: 130528.